

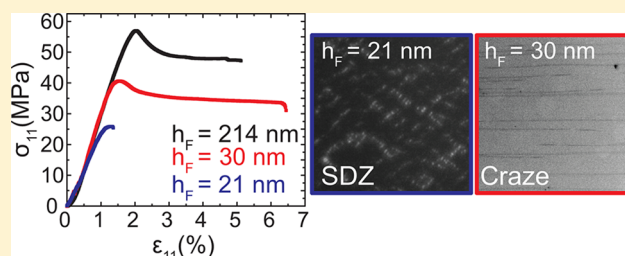
Confinement Effect on Strain Localizations in Glassy Polymer Films

R. Konane Bay,^b Shinichiro Shimomura, Yujie Liu, Mark Ilton, and Alfred J. Crosby*

Polymer Science and Engineering, University of Massachusetts, Amherst, Amherst, Massachusetts 01003, United States

Supporting Information

ABSTRACT: The physical properties of glassy polymer films change as they become confined. These changes are often attributed to increased average molecular mobility and reduction in entanglement density. Both are known to alter mechanical behavior, including the formation of strain localizations, e.g., crazing and shear deformation zones. Here, we determine how the entanglement density and surface mobility change the mechanical behavior of a glassy polymer film when it becomes confined. We utilize a custom-built uniaxial tensile tester for ultrathin films and dark-field optical microscopy to characterize the complete stress–strain response and the associated strain localizations for ultrathin polystyrene films of varying thickness ($h_F = 20$ –360 nm). These experiments provide direct measurement of the stress in a craze as well as the stresses involved through the transition from crazing to shear deformation zones. Most significantly, we observe a transition in strain localization from crazing to shear deformation zones as film thickness changes from 30 to 20 nm, providing new insights into how the surfaces alter the mechanical behavior in confined polymer films.



INTRODUCTION

Polymers play a dominant role in society due to their enabling properties. Molecular connectivity enables the same materials both to flow at elevated temperatures, taking on a seemingly infinite number of possible shapes for endless applications, and to resist stress and dissipate enormous energies to prevent failure at lower temperatures where devices operate. However, strikingly, these same mechanical attributes do not persist at small size scales. While other materials, e.g. inorganic glasses and metals, show a so-called “nanoeffect” with enhanced mechanical properties in ultrathin films,^{1–3} polymers suffer dramatic losses in mechanical strength in this state.⁴ Thus, current polymer materials are considered nearly unusable in applications that require mechanical integrity at decreased size scales. Why do these changes occur? Can new understanding allow this debilitating trend to be averted?

Structure and mobility change as glassy polymers are confined to dimensions that are less than their representative size scale in bulk materials.^{5–8} These changes have been discussed for close to 40 years, and over the past two decades there have been considerable experimental efforts to observe these changes. Understanding the changes in structure and mobility provides insight into how polymer properties develop. Following the scaling principles of de Gennes,⁶ Silberberg predicted that polymer molecules should be entropically constrained near a boundary, e.g., a free surface or rigid boundary, such that their random walk configuration will reflect upon itself more than an average molecule in the bulk.⁹ One consequence of this constraint is that molecules are not spherically symmetric on average, as in the bulk, but rather stretched in the plane of the neighboring boundary or surface. Several research groups have confirmed this prediction.^{10–12} A

second consequence is that sufficiently long polymer molecules near a surface are less entangled with neighboring molecules, as compared to counterparts in the bulk (Figure 1a). Although this consequence is significant because entanglements are critical for the development of a glassy polymer’s mechanical

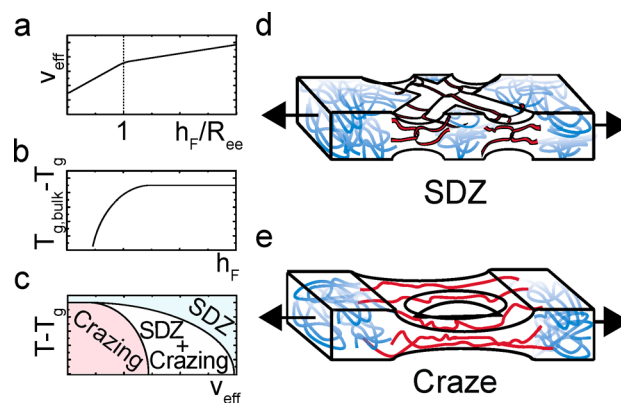


Figure 1. Schematic depiction of polystyrene thin film behavior (a) The entanglement density (v_{eff}) decreases with decreasing film thickness (adapted from ref 13). (b) The glass transition temperature decreases with decreasing film thickness (adapted from ref 16). (c) The strain localization transitions from crazing to shear deformation zones (SDZ) with increasing temperature and increasing entanglement density (adapted from ref 17). (d) Molecular scale diagram of a SDZ. (e) Molecular scale diagram of a craze with a void.

Received: February 19, 2018

Revised: April 26, 2018

Published: May 3, 2018

strength, there have been very limited studies, restricted to indirect methods, to observe and understand the implications of this loss of near-surface entanglements.^{5,13–15}

Beyond decreasing entanglements near a surface, glassy polymers change their relative mobility near free or constraining boundaries.^{5–8} For a model polymer such as polystyrene (PS), these changes give rise to an effective depression in the glass transition temperature, T_g , for molecules near a free surface (Figure 1b).^{16,18–24} One explanation of this depression is that the near-surface molecules are more mobile than molecules within the rest of the film,^{23,25,26} which can have dramatic impact on numerous properties, including their mechanical integrity.

From classical studies, it is well-known that glassy polymers decrease stiffness as temperature approaches T_g , i.e., segmental mobility increases.²⁷ More importantly, the manner in which glassy polymers fail changes significantly at elevated temperatures.²⁸ The yield strength, or stress at which polymer molecules move to a new permanent position, decreases with increasing temperature.²⁹ However, many glassy polymers, including the common example of PS, become more ductile, and effectively more “tough”, as temperatures approach the T_g .²⁸ This change from brittle to ductile behavior at a critical temperature is commonly called the ductile–brittle transition and is also observed in metals and ceramics. For polymers, there can be many reasons for this change, but one dominant mechanism for many common polymers is a change in how entangled polymer molecules “localize” strain as they are stressed globally. Strain localizations, including crazes and shear deformation zones (SDZ) which are most common for glassy polymers, control how polymer molecules respond to the activation of an applied stress. The overall system response of a given material always attempts to lower the total free energy; however, the path to lowering total energy can result in either distributed flow and dissipative processes, typically associated with SDZ (Figure 1d), or the drawing of nanofibrils/crazes (Figure 1e), which are often associated with the scission of backbone bonds and brittle fracture.^{28,30} For many common bulk glassy polymers, including PS, crazes occur at low temperatures while SDZ occur at elevated temperatures (Figure 1c).^{30,31} The density of intermolecular entanglements also affects the transition temperature. For polymers with greater entanglement density, the ductile–brittle, or SDZ-craze, transition is pushed to lower temperatures (Figure 1c), thus allowing more entangled glassy polymers to beneficially exhibit ductile and tough behavior over a wider temperature range.^{17,32} How do these critical localization processes manifest in polymer thin films where molecules near a surface or boundary play an increasingly important role? Does increased mobility lead to more ductile behavior? Does the loss of intermolecular entanglements favor embrittlement?

To answer these questions and provide new insight into how thin polymer materials respond to mechanical forces, we measure the uniaxial stress–strain response of PS films that range in thickness from 360 to 20 nm using an instrument and method that we recently introduced.⁴ We refer to this instrument as The Uniaxial Tensile Tester for Ultrathin films (TUTTUT). In our first description of this instrument, we were limited to measuring the properties of rectangular ultrathin films due to the intrinsic fragility of polystyrene films in the ultrathin state. Importantly, in this paper we report new processes to enable the manipulation and measurement of “dog-bone”-shaped films, thus preventing stress concentrations

and allowing strain localizations, such as crazes and SDZ to stabilize. This advance allows one of the first direct measurements of stresses within a crazed polymer film and, more significantly, the first observation of a thickness-controlled deformation transition. These measurements and their associated insights provide important fundamental lessons for how surfaces alter mechanical behavior of polymer glasses.

RESULTS AND DISCUSSION

To provide more insight into the thickness effect from surfaces on the mechanical behavior of glassy polymer films, we utilize an updated version of TUTTUT to directly measure the uniaxial stress–strain response (Figure 2a,b). Other researchers

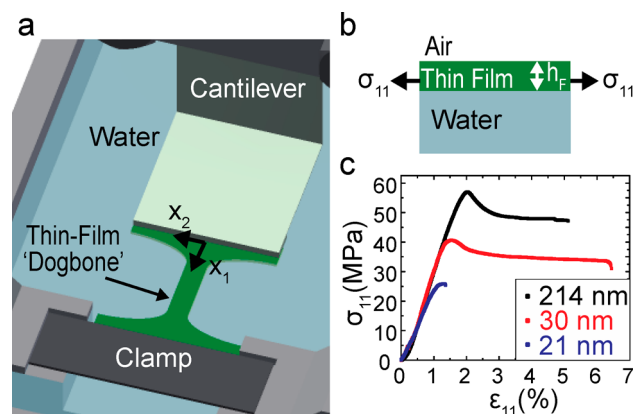


Figure 2. TUTTUT measurements of the complete stress–strain response demonstrates thickness-controlled mechanical property transitions. (a) Schematic of the uniaxial tensile tester for ultrathin films (TUTTUT). (b) Side view schematic of a dog-bone film being stretched on water. (c) Stress–strain response of three representative polystyrene (PS) films with decreasing thickness.

have used a load cell-based system to measure the stress–strain response of polymers^{33–36} and metal thin films;³⁷ however, the lowest thickness measured was 40 nm.³⁶ In this work, we use a cantilever-based system that allows for us to tune the force resolution to measure the stress–strain response of PS films as thin as 20 nm. The PS (Polymer Source, $M_w = 137$ kDa, $M_w/M_n = 1.05$) films are spin-coat from toluene solutions onto freshly cleaved mica. The spin-coating speed and solution concentration are varied to control the film thickness from 360 to 20 nm. The PS films are vacuum annealed at 170 °C for 25 min to remove solvent and residual stresses in the film. This annealing time is 530 times longer than the reptation time, $\tau_{rep} \cong 2.8$ s for the selected PS ($\tau_{rep} = A\tau(M_w)\tau(T)$, see the Supporting Information for full equation).³⁸ The annealing time was considered adequate based on a previous study, where annealing times of $\sim 170\tau_{rep}$ were found to be sufficient for removing residual stress.³⁹ The films are then laser-cut (Universal Laser Systems, VLS3.50) in a “dog-bone” shape to uniformly distribute the maximum stress into the gauge regime and eliminate stress concentrations at the grips (Figure S1). The films are then released onto a deionized water surface, and a silicon wafer is dropped on the grip section of the film. The water level is lowered, and the wafer positioned into the clamp and rigidly fixed onto the reservoir (Movie S1). A reflective cantilever (aluminum-coated cover glass) is attached to the other grip section of the film. An extension piece is attached to the cantilever to allow for a dark field microscope objective to

be fit into the setup. The entire reservoir is translated, and the cantilever deflection is measured. These deflections are calibrated for force sensing (force resolution $\sim 10 \mu\text{N}$) and displacement sensing (displacement resolution $\sim 1.4 \mu\text{m}$). Details on the calibration are provided in the [Experimental Section](#). The films are stretched at a constant velocity and thereby a fixed strain rate (0.0077 s^{-1}). We calculate the strain and stress from the measured force and displacement of the film, with details provided in the [Experimental Section](#).

Representative stress–strain responses of 300 to 20 nm thick PS films are provided in [Figure 2c](#) and [Figure S2](#). For all films, we observe an initial linear elastic stress–strain response followed by a yield response as strain localizations occur ([Movie S2](#) and [Movie S3](#)). For $h_F \geq 30 \text{ nm}$, crazes initiate prior to the critical yield stress and grow perpendicular to the primary stress direction. At the critical yield stress, the film exhibits a softening stress–strain response. After strain softening, the crazes continue to grow and widen and exhibit an “ideal perfectly plastic” behavior ($d\sigma/d\varepsilon = 0$). Most surprisingly, for 20 nm thick films, we observe a striking change in strain localization with the formation of SDZ. The SDZ are accompanied by a clear embrittlement, as indicated by the low values for critical yield stress and failure strain. To explain these thickness-controlled changes, we consider specific changes to five metrics: the observed strain localization morphology, elastic modulus, E , the failure strain, ε_{max} , critical yield stress, σ_{max} and the variance in ε_{max} .

We observe two transitions in strain localization morphology. As film thickness decreases, first, the craze structure changes from bulk crazes to a perforated sheet, or 2D craze morphology ([Figure 3](#)). Second, the strain localization process transitions from craze to SDZ ([Figure 3](#)). The first transition in structure from 3D bulk craze to the perforated structure has been previously reported,⁴⁰ and theoretically described.⁴¹ This first transition occurs when a film cannot develop stress normal to the film surfaces and has been observed for $h_F \leq 150 \text{ nm}$.⁴⁰ The second transition in strain localization morphology has not been previously observed. The transition from crazes in 30 nm thick films to SDZ in 20 nm thick films is the first observation of a thickness-controlled failure transition. The SDZ form initially 45° to the primary direction of stress, where the shear stress is maximum ([Figure S2](#)). However, the shear bands relax to 40° to the primary direction of the applied stress ([Figure 3](#), [Movie S3](#)). Furthermore, consistent with SDZ in bulk, we do not find any fibril formation in $h_F \sim 20 \text{ nm}$ strain localization zones, where in 30 nm thick PS films and 200 nm thick PS films, we observe crazes with the associated fibril formation ([Figure 3](#)).

To understand the thickness-controlled transition from craze to SDZ, we review similar transitions that have been observed in bulk glassy polymers. The transition from crazing to SDZ has been previously observed as the temperature approaches the T_g ([Figure 1c](#)).^{30,31} In this regime, this transition has been explained by increasing mobility of the polymer molecules causing a decreased stress barrier for yielding, σ_y , below the craze initiation stress, σ_c , leading to the formation of SDZ. Kramer and co-workers, based on the meniscus instability mechanism, proposed that σ_c is proportional to the square root of the yield stress ($\sigma_c \propto \sigma_y^{1/2}$); therefore, as temperature increases, the yield stress decreases at a faster rate than the crazing stress.³⁰

In addition to temperature, interchain entanglements are known to control the transition from craze to SDZ ([Figure](#)

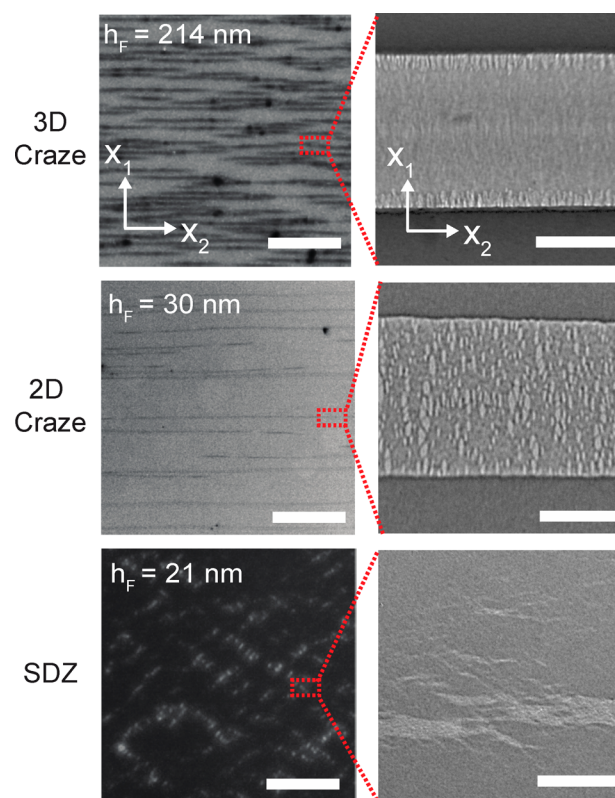


Figure 3. A transition from crazing to shear deformation zones (SDZ) is observed for polystyrene (PS) films $h_F \leq 20 \text{ nm}$ thick. (left) Dark-field optical microscopy images of the films after failure for three film thicknesses, h_F (scale bars are $250 \mu\text{m}$). The films with $h_F = 214 \text{ nm}$ and $h_F = 30 \text{ nm}$ exhibit crazes (images are inverted to enhance the contrast between craze and film), and $h_F = 21 \text{ nm}$ shows shear SDZs. (right) TEM images of strain localization for three film thicknesses, craze ($h_F = 214 \text{ nm}$, $h_F = 30 \text{ nm}$) and SDZ ($h_F = 21 \text{ nm}$) (scale bars are 500 nm).

[1c](#)).^{17,32} Craze formation is associated with low interchain entanglement density in glassy polymers and requires a loss of interchain entanglement, usually associated with disentanglement or chain scission.³⁰ As the interchain entanglement density increases, the average force per interchain entanglement decreases below the forces required for chain scission and forms SDZ.³⁰ Researchers have demonstrated that interchain entanglement density controls the craze–SDZ transition with cross-linking density,^{17,32} blends,⁴² and polymers with different entanglement densities.³²

In PS thin films, both average chain mobility^{5–8} and chain entanglements^{5,13–15} have been shown to be affected by film thickness. As a polymer film thickness decreases, higher fractions of molecules interact with the free surface, reducing the free volume at the surface.^{5–8} The surface layer has a higher chain mobility than the inner bulklike layer, which alters the physical properties of polymer films with decreasing thickness. The increase in mobility is often associated with the depression of T_g for PS ([Figure 1b](#)).^{16,18–24} Additionally, as thickness approaches the average polymer molecule size, the polymer chains interact more with themselves (intrachain entanglements) than their neighbors (interchain entanglements) ([Figure 1a](#)).⁹ The reduction in interchain entanglements leads to an increase in the average force per chain inducing early chain scission. As thickness decreases, the average chain

mobility increases, and the interchain entanglement density decreases.

To understand our observation, we propose a strain localization phase diagram where we plot temperature (T) versus h_F constructed with data points from previous classical studies on the SDZ–craze transition in bulk PS (Figure 4). At

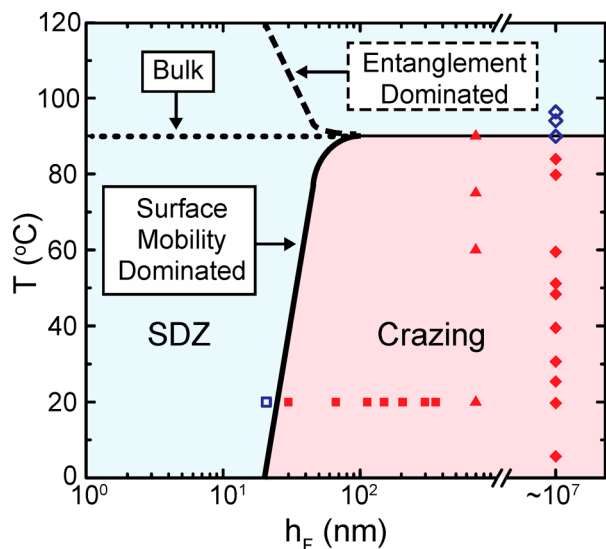


Figure 4. Predicted phase diagram as a function of film thickness h_F and temperature T . Red filled squares are film thicknesses where crazes form. Blue squares are the film thicknesses where shear deformation zones (SDZ) form. Red filled triangles are for 700 nm thick PS films from ref 17. Red filled diamonds are for PS tensile rods that form crazes, and blue diamonds are for PS tensile rods that form shear deformation zones from ref 28.

large thicknesses, the craze–SDZ transition occurs at high T near the PS bulk T_g .^{17,28} As thickness decreases, there are three possible paths for the strain localization behavior. The first path (represented by a dotted line) is proposed for materials where there is no effect from the entanglement density or surface mobility, i.e., follows the same craze–SDZ transition as bulk. The second path (represented by a dashed line) is proposed for materials where mobility is fixed or changing insignificantly. In this case, SDZ formation would be more difficult at lower h_F since the decrease in interchain entanglement would favor chain scission and associated craze formation at higher T . The third path (represented by a bold line) is proposed for materials where the effect of surface mobility change is more significant as compared to the effect of decreasing interchain entanglements. In this scenario, SDZ formation is more favorable at lower T , which is consistent with our observations for PS. Therefore, our observed transition from crazing to SDZ strongly suggests that the changes in surface mobility for PS thin films play a dominant role in the failure mechanisms of these materials in the confined state. Interestingly, we further note that the craze–SDZ transition in bulk PS occurs 10 °C below PS bulk T_g ²⁸ and we observe the transition 10 °C below the previously reported depressed average T_g for 20 nm thick free-standing PS films.²⁴

Furthermore, consistent with the influence of surface mobility on strain localization, we find E decreases at the film thicknesses where SDZ occur (Figure S3). We note $h_F = 20$ nm is below the average molecular size for the PS used ($M_w = 132$ kDa, the end-to-end distance, $R_{ee} = 25$ nm). This decrease is

consistent with our previous measurements⁴ as well as previous results measured using the surface wrinkling method,⁴³ however, these results are contradictory to what has been measured by other techniques for PS.^{44,45} Although the decrease in E has been associated with the higher volume fraction of near-surface molecules, there is a lack of agreement in the necessary size scales for the thickness dependence of E and the correlated depression in T_g . Therefore, an open question remains regarding what size scale leads to this decreased modulus in glassy polymers.

While we only observe one transition in E as a function of thickness, we observe two transitions in σ_{max} and ϵ_{max} that coincide with the two changes in strain localization morphologies, where σ_{max} is a more sensitive probe to these changes. For the 2D craze to SDZ morphology transition, we measure a sharp drop in σ_{max} from ~ 39 MPa for $h_F \sim 30$ nm to ~ 26 MPa for $h_F \sim 20$ nm (Figure 5). Even though σ_{max} of 20

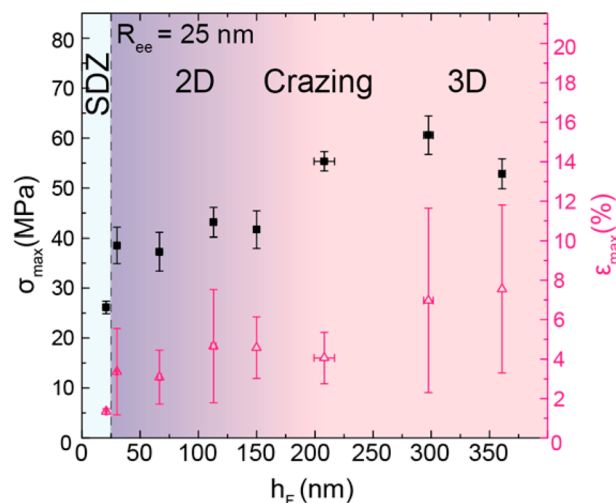


Figure 5. Thickness controls the transition in yield stress between strain localizations. Maximum stress, σ_{max} (black squares), and failure strain, ϵ_{max} (pink open triangles), as a function of film thickness, h_F . Error bars denote standard deviations for five independent films with the same thickness. Three regimes are marked: 3D crazing (pink), 2D crazing (purple), and shear deformation zones, SDZ (blue).

and 30 nm thick PS films have not been previously reported, the failure stress, $\sigma_{failure}$ for bulk PS films ($h_F \sim 208$ nm) is in agreement with previously $\sigma_{failure}$ values for bulk PS rods ($h_F \sim 10^7$ nm) at 20 °C where crazes form (Table S1).²⁸ Similarly, $\sigma_{failure}$ for 20 nm thick films are consistent with reported $\sigma_{failure}$ values where SDZ form in bulk PS rods at 90 °C.²⁸ In contrast with bulk PS measurements, we measure low $\epsilon_{max} \sim 1.3 \pm 0.1\%$ for $h_F = 20$ nm (Figure 5), which is unexpected since SDZ in bulk polystyrene are typically associated with “tough” or ductile behavior.²⁸ However, the decrease in ϵ_{max} is similar to the decrease in ϵ_{max} reported in our previous work.⁴ Accordingly, we associate this decrease with the loss of the interchain entanglements as h_F decreases, leading to an increased force per interchain entanglement and associated early chain scission leading to the embrittlement of the PS film. The tube diameter for PS is 8.5 nm,⁴⁶ and using our previous method to calculate the fraction of entanglements in the film,⁴ we estimate the force per entanglement to be 3.2 nN for a 20 nm thick film, which exceeds the force to break a PS backbone chain (3 nN).⁴⁷ Therefore, we propose that the 20 nm thick PS films undergo

early chain scission due to the loss in interchain entanglements, thus causing a significant decrease in the maximum yield stress and failure strain (Figure 5).

Similar to 2D craze to SDZ transition, we observe a decrease in σ_{\max} and ϵ_{\max} for the 3D craze to 2D craze transition (Figure 5). The decrease in σ_{\max} is consistent with previous work which has measured a decrease in true fibril stress.⁴⁰ Generally, in bulk PS, crazing is associated with brittle behavior with ϵ_{\max} around 1–4%.⁴⁸ For both the 2D craze and 3D craze polystyrene films, we measure ductile behavior with $\epsilon_{\max} = 4 \pm 2\%$ for 2D crazes ($30 \text{ nm} \leq h_F \leq 150 \text{ nm}$) and $\epsilon_{\max} = 8 \pm 4\%$ for 3D craze ($h_F > 150 \text{ nm}$) (Figure 5). We associate the ductile behavior with high craze stability. Kramer and co-workers measured similar craze stability with 400 nm thick PS films and noted stability dependence on defects.⁴⁹ This craze stability dependency accounts for the large variance in our measured ϵ_{\max} for films that crazed. The variance in ϵ_{\max} reduces in 20 nm thick PS films, where SDZ form and brittle behavior is observed (Figure 6). The decrease in variance provides an indirect technique to determine the changes in the strain localization morphology.

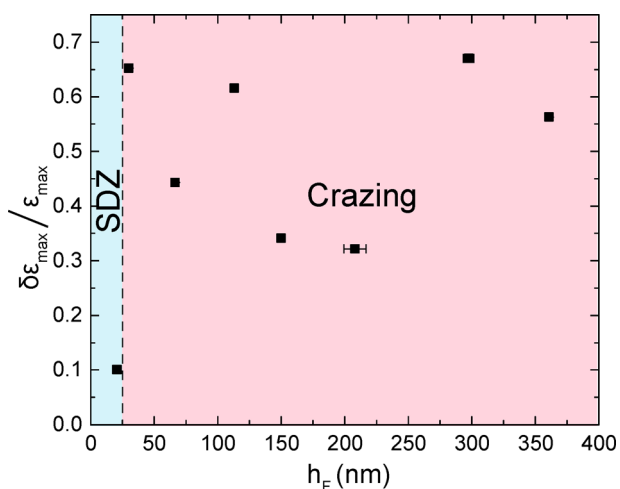


Figure 6. Transition from crazing to SDZ can be determined decrease in variance in the failure strain. Variance in failure strain $\delta\epsilon_{\max}/\epsilon_{\max}$ as a function of film thickness, h_F . Error bars denote standard deviations for five independent films with the same thickness. Two regimes are marked: 3D crazing (pink) and shear deformation zones, SDZ (blue).

Although TUTTUT provides an advance with regards to quantifying the complete stress–strain response of ultrathin polymer glasses, one question to consider is the possible effect of water. To address this question, we consider the conditions of our measurement and the findings of several previous studies. With regards to the possible role of surface tension on our measurements in our previous work, we showed that the elastic energy contribution dominates over the surface energy due to the PS film geometry being macroscale in two dimensions. Therefore, we neglect the surface energy contributions to the stress–strain response.⁴ Considering any possible concerns from swelling of the PS, the PS films are in contact with water for approximately 20 min, and previous work has shown that 60 nm PS films do not swell when in contact with water for 2 h.⁵⁰ However, in the work by Sasaki and co-workers, they reported a reduced surface mobile layer for PS spheres immersed in water⁵¹ compared to the mobile surface layer in free-standing films.⁵² This difference in the mobile surface layer could be possibly due to the conformation

changes of the pendant groups on the PS backbone.⁵⁰ With this being said, in both water and air, the measurements suggest that the surface chains have a higher mobility for PS.^{51,52} As discussed above, we hypothesize that the importance of this surface mobility for ultrathin films is associated with the thickness-controlled transition that we observe from crazes to SDZ. It would be interesting in the future to consider measurements of fully submerged and free-standing films to understand more details regarding the role of the surface mobile layer thickness on the ultrathin film mechanics. Overall, although we cannot eliminate the presence of water at this time, we do not consider it to be playing a significant role in our results. Moreover, we note that measuring the stress–strain response on a liquid bath provides the opportunities to investigate the effect of liquids, and liquid-born reactive species, on the mechanical properties of ultrathin glassy polymer films.

SUMMARY

In summary, we utilize TUTTUT and dark-field microscopy to directly measure and observe the thickness-controlled transitions in glassy polymer films. We provide a direct measurement of the stress in a 3D and 2D craze and the first observation of the transition in strain localization with decreasing thickness from crazing to SDZ. The transition from crazing to SDZ suggests that the increased average chain mobility plays a larger role than interchain entanglements in the strain localization behavior. However, we observe an embrittlement of polystyrene as the polymer film became confined, indicated by the decrease in failure strain and yield stress, which we attribute to a decrease in interchain entanglement density. Our findings indicate if interchain entanglement density is fixed with decreasing thickness, then SDZ will be stabilized, which is preferable for providing enhanced mechanical properties in an ultrathin film state.

EXPERIMENTAL SECTION

Materials. We utilized PS purchased from Polymer Source (weight-average molecular weight $M_w = 132\,000 \text{ g/mol}$, dispersity $M_w/M_n = 1.05$). Toluene solutions of PS (0.6–5.5 wt %) were spin-cast (2000–4000 rpm) onto freshly cleaved mica sheet to fabricate the films. The PS films were vacuum annealed at 170 °C for 25 min. The 150 nm thick PS films were vacuum annealed 130 °C for 24 h. The films were slowly cooled (0.4 °C/min) under vacuum. The films were laser-cut (Universal Laser System VSL3.5) at 3% power, 40% speed, and a points per inch of 706. The gauge length of the films was 7.62 mm and width was 3.1 mm; the geometry can be seen in Figure S1.

Floating Thin Polymer Films on Water. Films were floated from the mica onto the surface of a water bath. We dropped a silicon wafer cut into a rectangle (34 mm × 8 mm) onto the grip section of the “dog-bone” film. The water level was lowered, and the wafer was positioned into the clamp and rigidly fixed onto the water bath (Movie S1). We aligned the film edge with the extension piece on the cantilever and raised the reservoir to place the other grip section in contact with the extension piece.

Thickness and Gauge Length Determination. After the film is attached to both sides, the extra material from the sides is picked up with a cleaned silicon wafer (washed by sonication in soap water, acetone, toluene, and isopropanol) for thickness, h_F measurement with ellipsometry (PS refractive index, $n_{PS} = 1.59$). We calculated gauge length, L_g , from measured distance between grips (L_r) using the equation $L_g = (L_r - 16.6)^{0.74} + 14.5$, which was developed from FEA model for our “dog-bone” geometry (Figure S1).

Video Capture and Detection. The laser point was directed from a helium neon laser system (ThorLabs HGR005) at wavelength of 543 nm with beam diameter of 0.64 mm. Experiments were conducted

after waiting 30 min for the laser system to warm up. Laser point movement was captured using a DSLR camera (Nikon D5300) with resolution of 1920×1080 pixels, and the macroscopic deformation of the film was captured with another DSLR camera (Nikon D5500) with resolution 1920×1080 pixels. The frame rate was chosen to be 60 fps for both cameras. The dark-field microscopy of the deformations in the film was captured using a zoom tube with an attached fiber-optic ring light and microscope camera (PixelINK-B776U) with resolution 1920×1080 pixels. The frame rate was chosen to be 10 fps. The laser point was tracked by identifying the center of mass then fitting the laser point intensity with a Gaussian distribution in each frame. From this we determined the pixel displacement versus time. Using the two cantilever calibrations, and the initial geometry of the film, we converted displacement versus time to a stress versus strain.

Cantilever Calibration. For the force calibration (mN/pixel), we utilized the stiffness of the cantilever. The stiffness of the cantilever was calculated by measuring the fundamental resonance frequency of the cantilever at varying lengths. The cantilever was tapped, and the laser point reflected onto a white screen. The laser points oscillations were recorded with a high-speed camera (FASTCAM SA3) from 3000 to 6000 fps depending on the length of the cantilever. The laser point was tracked with the same method as mentioned previously, and we fit a Fourier transform to find the frequency (Figure S4). From the frequency (f), length of the cantilever (L_c), total length of the cantilever (L_{total}), and total mass of the cantilever (m_{total}), we calculated the stiffness of the cantilever (S_c) by $S_c = \frac{12\pi^2 f^2}{3.52^2} m_{total} \frac{L_c}{L_{total}}$.⁵³ For the displacement calibration ($\mu\text{m}/\text{pixel}$), a white screen was placed to reach the maximum pixel displacement for the maximum force estimated for a given film thickness. A known displacement was applied in the x_1 direction, and the pixel displacement was determined. Using image analysis, a linear fit was applied, and the resulting slope (m_1) was the calibration for the cantilever displacement (μm) per pixel (Figure S4). Using m_1 , the force calibration (m_2) was calculated using the stiffness of the cantilever, $m_2 = m_1 S_{cant}$. The cantilever displacement (δ_{cant}) was calculated from the laser point pixel displacement divided by the slope, m_1 , and the total displacement (δ_{total}) was calculated from the linear actuator velocity multiplied by the time. The film displacement (δ_{film}) is equal to the cantilever displacement (δ_{cant}) subtracted from total displacement (δ_{total}), and we determined the strain ($\epsilon_{11} = \delta_{film}/L_{film}$) by dividing the film displacement by the initial length between the grips. We have verified the global strains match the local strain measured from dark-field micrographs. The force (F_{film}) is calculated by dividing the laser point pixel displacement by m_2 . The stress on the film ($\sigma_{11} = F_{film}/h_F w_F$) is calculated by dividing the force by the thickness of the film and the width of the gauge.

TEM Sample Preparation. Films were stretched to 2.5% strain for $h_F \sim 30$ nm and $h_F \sim 210$ nm and to 0.8% for $h_F \sim 20$ nm in TUTTUT with a rigid 3D printed cantilever at the same strain rate as stress-strain experiments (0.0077 s^{-1}). A TEM copper grid with a 2 mm aperture coated in PS (to promote adhesion of the film and copper grid) was dropped onto the stretched gauge regime of the film. The grid and film were then picked off the water bath surface and mounted into the TEM sample holder. Images were taken by a JEOL 2000FX under 200 keV acceleration voltage.

■ ASSOCIATED CONTENT

Supporting Information

The Supporting Information is available free of charge on the ACS Publications website at DOI: 10.1021/acs.macromol.8b00385.

Figures S1–S4 and Table S1 (PDF)

Movie S1 (MOV)

Movie S2 (MOV)

Movie S3 (MOV)

■ AUTHOR INFORMATION

Corresponding Author

*E-mail: acrosby@umass.edu (A.J.C.).

ORCID

R. Konane Bay: 0000-0002-3980-8491

Notes

The authors declare no competing financial interest.

■ ACKNOWLEDGMENTS

We acknowledge financial support from the National Science Foundation (DMR 1608614) and Northeast Alliance for Graduate Education and Professoriate at the University of Massachusetts Amherst (NEAGAP).

■ REFERENCES

- (1) Haque, M. A.; Saif, M. T. A. In-Situ Tensile Testing of Nano-Scale Specimens in SEM and TEM. *Exp. Mech.* **2002**, *42* (1), 123–128.
- (2) Gruber, P. A.; Böhm, J.; Onuseit, F.; Wanner, A.; Spolenak, R.; Arzt, E. Size Effects on Yield Strength and Strain Hardening for Ultra-Thin Cu Films with and without Passivation: A Study by Synchrotron and Bulge Test Techniques. *Acta Mater.* **2008**, *56*, 2318–2335.
- (3) Chu, J. P.; Jang, J. S. C.; Huang, J. C.; Chou, H. S.; Yang, Y.; Ye, J. C.; Wang, Y. C.; Lee, J. W.; Liu, F. X.; Liaw, P. K.; Chen, Y. C.; Lee, C. M.; Li, C. L.; Rullyani, C. Thin Film Metallic Glasses: Unique Properties and Potential Applications. *Thin Solid Films* **2012**, *520*, 5097–5122.
- (4) Liu, Y.; Chen, Y.-C.; Hutchens, S.; Lawrence, J.; Emrick, T.; Crosby, A. J. Directly Measuring the Complete Stress–Strain Response of Ultrathin Polymer Films. *Macromolecules* **2015**, *48* (18), 6534–6540.
- (5) Brown, H. R.; Russell, T. P. Entanglements at Polymer Surfaces and Interfaces. *Macromolecules* **1996**, *29*, 798–800.
- (6) de Gennes, P. G. *Scaling Concepts in Polymer Physics*; Cornell University Press: Ithaca, NY, 1979.
- (7) de Gennes, P. G. Glass Transitions in Thin Polymer Films. *Eur. Phys. J. E: Soft Matter Biol. Phys.* **2000**, *2* (3), 201–205.
- (8) Ediger, M. D.; Forrest, J. A. Dynamics near Free Surfaces and the Glass Transition in Thin Polymer Films: A View to the Future. *Macromolecules* **2014**, *47* (2), 471–478.
- (9) Silberberg, A. Distribution of Conformations and Chain Ends near the Surface of a Melt of Linear Flexible Macromolecules. *J. Colloid Interface Sci.* **1982**, *90* (1), 86–91.
- (10) Jones, R. L.; Kumar, S. K.; Ho, D. L.; Briber, R. M.; Russell, T. P. Chain Conformation in Ultrathin Polymer Films Using Small-Angle Neutron Scattering. *Macromolecules* **2001**, *34*, 559–567.
- (11) Jones, R. L.; Kumar, S. K.; Ho, D. L.; Briber, R. M.; Russell, T. P. Chain Conformation in Ultrathin Polymer Films. *Nature* **1999**, *400*, 146–149.
- (12) Jones, R. L.; Soles, C. L.; Starr, F. W.; Lin, E. K.; Lenhart, J. L.; Wu, W.; Goldfarb, D. L.; Angelopoulos, M. Chain Conformation in Ultrathin Polymer Films. In *SPIE, 19th Annual Conference on Advances in Resist Technology and Processing*; 2002; pp 342–350.
- (13) Si, L.; Massa, M. V.; Dalnoki-Veress, K.; Brown, H. R.; Jones, R. A. L. Chain Entanglement in Thin Freestanding Polymer Films. *Phys. Rev. Lett.* **2005**, *94*, 127801.
- (14) Baumchen, O.; Fetzer, R.; Jacobs, K. Reduced Interfacial Entanglement Density Affects the Boundary Conditions of Polymer Flow. *Phys. Rev. Lett.* **2009**, *103* (24), 1–4.
- (15) Rathfon, J. M.; Cohn, R. W.; Crosby, A. J.; Rothstein, J. P.; Tew, G. N. Confinement Effects on Chain Entanglement in Free-Standing Polystyrene Ultrathin Films. *Macromolecules* **2011**, *44* (13), 5436–5442.
- (16) Keddie, J. L.; Jones, R. A. L.; Cory, R. A. Size-Dependent Depression of the Glass Transition Temperature in Polymer Films. *Europhys. Lett.* **1994**, *27* (1), 59–64.

- (17) Berger, L. L.; Kramer, E. J. The Effect of Temperature on the Transition from Crazing to Shear Deformation in Crosslinked Polystyrene. *J. Mater. Sci.* **1988**, *23*, 3536–3543.
- (18) Gao, S.; Koh, Y. P.; Simon, S. L. Calorimetric Glass Transition of Single Polystyrene Ultrathin Films. *Macromolecules* **2013**, *46* (2), 562–570.
- (19) Forrest, J. A.; Dalnoki-Veress, K.; Stevens, J. R.; Dutcher, J. R. Effect of Free Surfaces on the Glass Transition Temperature of Thin Polymer Films. *Phys. Rev. Lett.* **1996**, *77* (10), 2002–2005.
- (20) Forrest, J. A.; Dalnoki-Veress, K.; Dutcher, J. R. Interface and Chain Confinement Effects on the Glass Transition Temperature of Thin Polymer Films. *Phys. Rev. E: Stat. Phys., Plasmas, Fluids, Relat. Interdiscip. Top.* **1997**, *56* (5), 5705–5716.
- (21) Ellison, C. J.; Torkelson, J. M. The Distribution of Glass-Transition Temperatures in Nanoscopically Confined Glass Formers. *Nat. Mater.* **2003**, *2* (10), 695–700.
- (22) Fakhraai, Z.; Still, T.; Fytas, G.; Ediger, M. D. Structural Variations of an Organic Glassformer Vapor-Deposited. *J. Phys. Chem. Lett.* **2011**, *2*, 423–427.
- (23) Yang, Z.; Fujii, Y.; Lee, F. K.; Lam, C.; Tsui, O. K. C. Glass Transition Dynamics and Surface Layer Mobility in Unentangled Polystyrene Films. *Science (Washington, DC, U. S.)* **2010**, *328*, 1676–1679.
- (24) Mattsson, J.; Forrest, J. A.; Börjesson, L. Quantifying Glass Transition Behavior in Ultrathin Free-Standing Polymer Films. *Phys. Rev. E: Stat. Phys., Plasmas, Fluids, Relat. Interdiscip. Top.* **2000**, *62* (4), 5187–5200.
- (25) Chai, Y.; Salez, T.; Mcgraw, J. D.; Benzaquen, M.; Dalnoki-veress, K.; Raphael, E.; Forrest, J. A. A Direct Quantitative Measure of Surface Mobility in a Glassy Polymer. *Science (Washington, DC, U. S.)* **2014**, *343*, 994–999.
- (26) Fakhraai, Z.; Forrest, J. A. Measuring the Surface Dynamics of Glassy Polymers. *Science (Washington, DC, U. S.)* **2008**, *319*, 600–605.
- (27) Ward, I. M.; Hadley, D. W. *An Introduction to the Mechanical Properties of Solid Polymers*; 1993.
- (28) Matsushige, K.; Radcliffe, S. V.; Baer, E. The Pressure and Temperature Effects on Brittle-to-Ductile Transition in PS and PMMA. *J. Appl. Polym. Sci.* **1976**, *20*, 1853–1866.
- (29) Eyring, H. Viscosity, Plasticity, and Diffusion as Examples of Absolute Reaction Rates. *J. Chem. Phys.* **1936**, *4* (4), 283–291.
- (30) Kramer, E. J. Craze Fibril Formation and Breakdown. *Polym. Eng. Sci.* **1984**, *24* (10), 761–769.
- (31) Berger, L. L.; Kramer, E. J. Chain Disentanglement during High-Temperature Crazing of Polystyrene. *Macromolecules* **1987**, *20*, 1980–1985.
- (32) Henke, C. S.; Kramer, E. J. Crazing and Shear Deformation in Crosslinked Polystyrene. *J. Polym. Sci., Polym. Phys. Ed.* **1984**, *22*, 721–737.
- (33) Kim, T.; Kim, J.-H.; Kang, T. E.; Lee, C.; Kang, H.; Shin, M.; Wang, C.; Ma, B.; Jeong, U.; Kim, T.-S.; Kim, B. J. Flexible, Highly Efficient All-Polymer Solar Cells. *Nat. Commun.* **2015**, *6*, 8547.
- (34) Kim, J.-H.; Noh, J.; Choi, H.; Lee, J.-Y.; Kim, T.-S. Mechanical Properties of Polymer–Fullerene Bulk Heterojunction Films: Role of Nanomorphology of Composite Films. *Chem. Mater.* **2017**, *29*, 3954–3961.
- (35) Kim, J. S.; Kim, J. H.; Lee, W.; Yu, H.; Kim, H. J.; Song, I.; Shin, M.; Oh, J. H.; Jeong, U.; Kim, T. S.; Kim, B. J. Tuning Mechanical and Optoelectrical Properties of Poly(3-Hexylthiophene) through Systematic Regioregularity Control. *Macromolecules* **2015**, *48* (13), 4339–4346.
- (36) Hasegawa, H.; Ohta, T.; Ito, K.; Yokoyama, H. Stress-Strain Measurement of Ultra-Thin Polystyrene Films: Film Thickness and Molecular Weight Dependence of Crazing Stress. *Polymer* **2017**, *123*, 179–183.
- (37) Kim, J.; Nizami, A.; Hwangbo, Y.; Jang, B.; Lee, H.; Woo, C.; Hyun, S.; Kim, T. Tensile Testing of Ultra-Thin Films on Water Surface. *Nat. Commun.* **2013**, *4*, 1–6.
- (38) Mcgraw, J. D.; Jago, N. M.; Dalnoki-veress, K. Capillary Levelling as a Probe of Thin Film Polymer Rheology. *Soft Matter* **2011**, *7*, 7832–7838.
- (39) Chung, J. Y.; Chastek, T. Q.; Fasolka, M. J.; Ro, H. W.; Stafford, C. M. Quantifying Residual Stress in Nanoscale Thin Polymer Films via Surface Surface Wrinkling. *ACS Nano* **2009**, *3* (4), 844–852.
- (40) Chan, T.; Donald, A. M.; Kramer, E. J. Film Thickness Effects on Craze Micro Mechanics. *J. Mater. Sci.* **1981**, *16*, 676–686.
- (41) Krupenkin, T. N.; Fredrickson, G. H. Crazing in Two and Three Dimensions. 1. Two-Dimensional Crazing. *Macromolecules* **1999**, *32*, 5029–5035.
- (42) Donald, A. M.; Kramer, E. J. The Competition between Shear Deformation and Crazing in Glassy Polymers. *J. Mater. Sci.* **1982**, *17* (7), 1871–1879.
- (43) Stafford, C. M.; Vogt, B. D.; Harrison, C.; Julthongpipit, D.; Huang, R. Elastic Moduli of Ultrathin Amorphous Polymer Films. *Macromolecules* **2006**, *39* (15), 5095–5099.
- (44) O’Connell, P. A.; McKenna, G. B. Dramatic Stiffening of Ultrathin Polymer Films in the Rubbery Regime. *Eur. Phys. J. E: Soft Matter Biol. Phys.* **2006**, *20* (2), 143–150.
- (45) Chung, P. C.; Glynos, E.; Green, P. F. The Elastic Mechanical Response of Supported Thin Polymer Films. *Langmuir* **2014**, *30*, 15200–15205.
- (46) Rubinstein, M.; Colby, R. H. *Polymer Physics*; Oxford University Press: 2003.
- (47) Kausch, H. H. *Polymer Fracture*; Springer: Berlin, 1978.
- (48) *Physical Properties of Polymers Handbook*; Mark, J. E., Ed.; AIP Press: Woodbury, NY, 1996.
- (49) Yang, A. C.; Kramer, E. J.; Kuo, C. C.; Phoenix, S. L. Craze Fibril Stability and Breakdown in Polystyrene. *Macromolecules* **1986**, *19*, 2010–2019.
- (50) Horinouchi, A.; Yamada, N. L.; Tanaka, K. Aggregation States of Polystyrene at Nonsolvent Interfaces. *Langmuir* **2014**, *30*, 6565–6570.
- (51) Sasaki, T.; Shimizu, A.; Mourey, T. H.; Thureau, C. T.; Ediger, M. D. Glass Transition of Small Polystyrene Spheres in Aqueous Suspensions Glass Transition of Small Polystyrene Spheres in Aqueous Suspensions. *J. Chem. Phys.* **2003**, *119*, 8730.
- (52) Paeng, K.; Swallen, S. F.; Ediger, M. D. Direct Measurement of Molecular Motion in Freestanding Polystyrene Thin Films. *J. Am. Chem. Soc.* **2011**, *133*, 8444–8447.
- (53) Ashby, M. F. *Materials Selection in Mechanical Design*, 4th ed.; Elsevier Ltd.: Burlington, 2011.